Medjunarodni naučno-stručni skup sa izložbom
XXIII NAUKA I MOTORNA VOZILA SCIENCE AND MOTOR VEHICLES 2011
International Automotive Conference with Exhibition
19 - 21 April 2011, Beograd, Serbia

NMV11AETT07

Influence on the Dynamic Behavior of Full Car Equipped by Magnetorheological Damper via Switch on/off and h_∞ Controller

G. Barbaraci; G. Virzi' Mariotti
Dipartimento di Ingegneria Industriale, Università di Palermo, Italy


Abstract. This paper shows the influence on dynamic behavior of the car when it is equipped with magneto-rheological dampers controlled by a feedback. The feedback is built up in two ways; the first is implemented by a switch on/off control that is characterized by the injection of magnetic field with a constant value. It happens when a certain value of relative speed between the sprung and unsprung mass is exceeded. The second feedback is characterized by the H-infinity control which is based on the relative displacement in order to vary the magnetic field signal in a continuous manner. At the same time the H-infinity control of vehicle is maintained by taking into account the exceeding of speed signal in order to consider the substantial differences with the switch on/off control. These differences are evaluated in terms of relative displacement and speed between the unsprung and sprung mass. The exogenous excitation is the road disturbances which are introduced as a square wave input in order to emulate those that are commonly encountered on the road. All simulations and results are performed by MATLab-Simulink and Mathematica.

Keywords: Full car, magneto-rheological fluids, shock absorber, control systems.

1. INTRODUCTION

Magneto-Rheological (MR) dampers have taken over the last decade an important role in research in mechanical design. Their use is justified by the numerous publications characterizing the landscape of scientific research in order to obtain a validation of experimental results, with the contribution of additional road safety in the automotive field. There are a certain number of applications of magneto-rheological dampers. In the automotive a set of design and experimental studies were performed in order to validate the advantages by investigations about optimizing the dynamic response in an experimental way [1] using a small amount of energy to produce a large controllable damping force. Their applications covered the aeronautical field about the design of landing gear [2] where an approach focused on the impact during the landing phase of an aircraft flight subjected to a large variations in sink speed and aircraft mass under different angle of attack.
..

The experimental verification of [2] is performed by an implementation of semi-active damping using a magneto-rheological fluid [3]. A further investigation on aeronautical field considers the lag mode damping in helicopters, so that damping requirements can be varied as a function of different flight conditions [4]. A magneto-rheological fluid-elastomeric (MRFE) is used in the helicopter application. Magneto-rheological dampers have the advantages of a lower consumption of energy than electro-rheological (ER) ones. This is due to the fact that electro-rheological fluids need to separate the electric charge from a plate to one in an opposite side of a condenser. This separation needs high voltage while magneto-rheological fluid need only to spread magnetic field flux implemented by a lower energy than electro-rheological one. Although there is a discrepancy in the energy consumption between MR and ER-fluids, this last represent an elegant means of providing continuously variable forces for the control of mechanical vibration [5]. Both MR and ER-fluids technology are related by a non linear behavior which can make difficult the prediction of their performance, particularly when they are integrated into engineering structures [6]. An example is a building subjected to a seismic excitation equipped by MR-fluids damper activated by a feedback variable in order to produce the control vibration input thanks to the control system [7]. MR damper is a powerful tool to improve the operating performance when the structural vibration has high intensity in transmitting the external force, like in the case of the weapon system, where the damping of the recoil effect is necessary to attenuate the vibration of all structure supporting it [8].

NOMENCLATURE

$z_s(t)$ Vertical displacement of the frame

$z_{sfr}(t)$ Front Right sprung mass displacement

$z_{sfl}(t)$ Front left sprung mass displacement

$z_{srr}(t)$ Rear right sprung mass displacement

$z_{srl}(t)$ Rear left sprung mass displacement

$z_{ufr}(t)$ Front right unsprung mass displacement

$z_{ufl}(t)$ Front left unsprung mass displacement

$z_{urr}(t)$ Rear right unsprung mass displacement

$z_{url}(t)$ Rear left unsprung mass displacement

$\mathbf{T}$ Matrix of coordinate transformations

$q_s(t)$ Vector of controlled displacements

$q(t)$ Vector of controlled displacements

$\mathbf{d}_n(t)$ Road disturbance vector

F_{fr} Front right magneto-rheological force

F_{fl} Front left magneto-rheological force

F_{rr} Rear right magneto-rheological force

F_{rl} Rear left magneto-rheological force

$\mathbf{I}$ Identity matrix

$\alpha(t)$ Pitch angle

$\beta(t)$ Roll angle

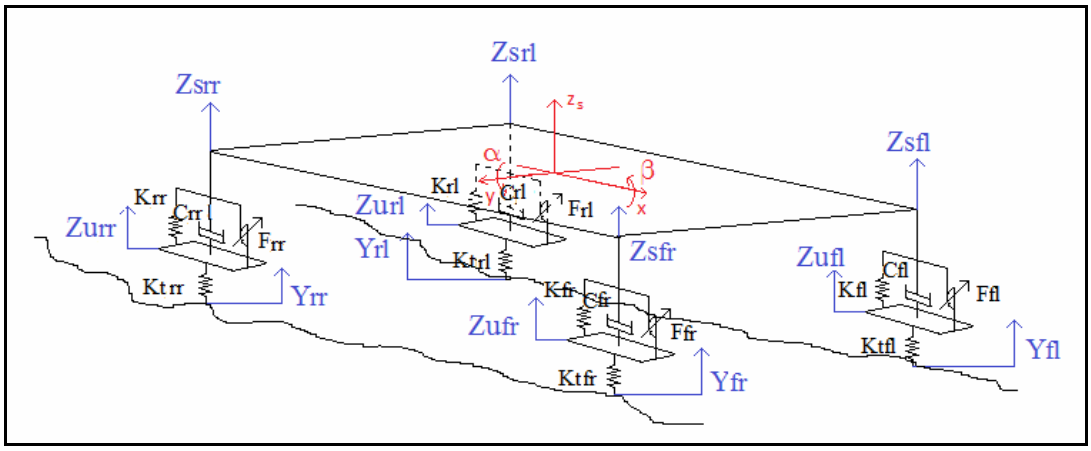

Fig. 1: Schematic view of full car.

2 MATHEMATICAL MODEL

The full car mathematical model is carried out according to figure 1, that is similar to the system described in [9]. In the same figure the vehicle is sketched by five masses, four tires and the chassis; the last is represented by the greatest rectangle.

The components of suspension system are characterized by mechanical spring, passive damping and magneto-rheological damper. All bodies are rigid in order to avoid a further complication of vibration analysis and mathematical model. A linear relation is established between the displacements of all points belonging to the chassis and the point where the shock absorber is located [10]. The road disturbance is characterized by the vector $\mathbf{y}(t)$ which contains four components: each of them acts on one tire; this doesn't have a damping effect but only a spring with a linear behavior. Consequently to the acceleration of the wheel, the force is injected in the point of the chassis where the suspension system is located. This force produces some motion effects which lead the vehicle to three kind of displacements: translation along z_s, rotation along x and y directions; these two last are measured by the angles α and β of a frame with the origin on chassis's center of mass. Each shock-absorber is sketched as a two degree of freedom damped system. Their presence in a number of four leads to an uncoupled matrix differential equation:

$$\begin{bmatrix} m_{fr} & 0 & 0 & 0 \\ 0 & m_{fl} & 0 & 0 \\ 0 & 0 & m_{rr} & 0 \\ 0 & 0 & 0 & m_{rl} \end{bmatrix} \begin{bmatrix} \ddot{z}_{fr} \\ \ddot{z}_{fl} \\ \ddot{z}_{rr} \\ \ddot{z}_{rl} \end{bmatrix} + \begin{bmatrix} c_{fr} & 0 & 0 & 0 \\ 0 & c_{fl} & 0 & 0 \\ 0 & 0 & c_{rr} & 0 \\ 0 & 0 & 0 & c_{rl} \end{bmatrix} \begin{bmatrix} \dot{z}_{fr} \\ \dot{z}_{fl} \\ \dot{z}_{rr} \\ \dot{z}_{rl} \end{bmatrix} + \begin{bmatrix} k_{fr}+k_{tfr} & 0 & 0 & 0 \\ 0 & k_{fl}+k_{tfl} & 0 & 0 \\ 0 & 0 & k_{rr}+k_{trr} & 0 \\ 0 & 0 & 0 & k_{rl}+k_{trl} \end{bmatrix} \begin{bmatrix} z_{ufr} \\ z_{ufl} \\ z_{urr} \\ z_{url} \end{bmatrix} = \begin{bmatrix} c_{fr} & 0 & 0 & 0 \\ 0 & c_{fl} & 0 & 0 \\ 0 & 0 & c_{rr} & 0 \\ 0 & 0 & 0 & c_{rl} \end{bmatrix} \begin{bmatrix} \dot{z}_{sfr} \\ \dot{z}_{sfl} \\ \dot{z}_{srr} \\ \dot{z}_{srl} \end{bmatrix} + \begin{bmatrix} k_{fr} & 0 & 0 & 0 \\ 0 & k_{fl} & 0 & 0 \\ 0 & 0 & k_{rr} & 0 \\ 0 & 0 & 0 & k_{rl} \end{bmatrix} \begin{bmatrix} z_{sfr} \\ z_{sfl} \\ z_{srr} \\ z_{srl} \end{bmatrix} + \begin{bmatrix} k_{tfr} & 0 & 0 & 0 \\ 0 & k_{tfl} & 0 & 0 \\ 0 & 0 & k_{trr} & 0 \\ 0 & 0 & 0 & k_{trl} \end{bmatrix} \begin{bmatrix} y_{fr} \\ y_{fl} \\ y_{rr} \\ y_{rl} \end{bmatrix} - \begin{bmatrix} F_{fr} \\ F_{fl} \\ F_{rr} \\ F_{rl} \end{bmatrix} \quad (1)$$

Chassis's motion equation is performed according to the variables of vertical displacements and rotation along x and y direction and it is characterized by three coupled differential equations:

$$\begin{bmatrix} m_s & 0 & 0 \\ 0 & I_y & 0 \\ 0 & 0 & I_x \end{bmatrix}\begin{bmatrix} \ddot{z} \\ \ddot{\alpha} \\ \ddot{\beta} \end{bmatrix}+\begin{bmatrix} c_{fr} & c_{fl} & c_{rr} & c_{rl} \\ -c_{fr}b & -c_{fl}b & c_{rr}a & c_{rl}a \\ c_{fr}c & -c_{fl}d & c_{rr}c & -c_{rl}d \end{bmatrix}\begin{bmatrix} \dot{z}_{sfr} \\ \dot{z}_{sfl} \\ \dot{z}_{srr} \\ \dot{z}_{srl} \end{bmatrix}+\begin{bmatrix} k_{fr} & k_{fl} & k_{rr} & k_{rl} \\ -k_{fr}b & -k_{fl}b & k_{rr}a & k_{rl}a \\ k_{fr}c & -k_{fl}d & k_{rr}c & -k_{rl}d \end{bmatrix}\begin{bmatrix} z_{sfr} \\ z_{sfl} \\ z_{srr} \\ z_{srl} \end{bmatrix}=\begin{bmatrix} c_{fr} & c_{fl} & c_{rr} & c_{rl} \\ -c_{fr}b & -c_{fl}b & c_{rr}a & c_{rl}a \\ c_{fr}c & -c_{fl}d & c_{rr}c & -c_{rl}d \end{bmatrix}\begin{bmatrix} \dot{z}_{ufr} \\ \dot{z}_{ufl} \\ \dot{z}_{urr} \\ \dot{z}_{url} \end{bmatrix}+$$
$$+\begin{bmatrix} k_{fr} & k_{fl} & k_{rr} & k_{rl} \\ -k_{fr}b & -k_{fl}b & k_{rr}a & k_{rl}a \\ k_{fr}c & -k_{fl}d & k_{rr}c & -k_{rl}d \end{bmatrix}\begin{bmatrix} z_{ufr} \\ z_{ufl} \\ z_{urr} \\ z_{url} \end{bmatrix}+\begin{bmatrix} 1 & 1 & 1 & 1 \\ -b & -b & a & a \\ c & -d & c & -d \end{bmatrix}\begin{bmatrix} F_{fr} \\ F_{fl} \\ F_{rr} \\ F_{rl} \end{bmatrix} \tag{2}$$

the previous (1) and (2) are written in a symbolic way in (3) and (4):

$$\mathbf{M}_u\ddot{\mathbf{q}}_u(t)+\mathbf{C}_u\dot{\mathbf{q}}_u(t)+(\mathbf{K}_u+\mathbf{K}_t)\mathbf{q}_u(t)=\mathbf{C}_u\dot{\mathbf{q}}_s(t)+\mathbf{K}_u\mathbf{q}_s(t)+\mathbf{K}_t\mathbf{y}(t)-\mathbf{F}_{MR} \tag{3}$$

$$\mathbf{M}_s\ddot{\mathbf{q}}_s(t)+\mathbf{C}_s\dot{\mathbf{q}}_s(t)+\mathbf{K}_s\mathbf{q}_s(t)=\mathbf{C}_s\dot{\mathbf{q}}_u(t)+\mathbf{K}_s\mathbf{q}_u(t)+\mathbf{T}^T\mathbf{F}_{MR} \tag{4}$$

The entire dynamic behavior is characterized by seven coupled linear differential equations of the second order, with constant coefficients non homogenous:

$$\begin{bmatrix} \ddot{\mathbf{q}}_s(t) \\ \ddot{\mathbf{q}}_u(t) \end{bmatrix}=\begin{bmatrix} -\mathbf{M}_s^{\dagger}\mathbf{C}_s & \mathbf{M}_s^{\dagger}\mathbf{C}_s \\ \mathbf{M}_u^{-1}\mathbf{C}_u & -\mathbf{M}_u^{-1}\mathbf{C}_u \end{bmatrix}\begin{bmatrix} \dot{\mathbf{q}}_s(t) \\ \dot{\mathbf{q}}_u(t) \end{bmatrix}+\begin{bmatrix} -\mathbf{M}_s^{\dagger}\mathbf{K}_s & \mathbf{M}_s^{\dagger}\mathbf{K}_s \\ \mathbf{M}_u^{-1}\mathbf{K}_u & -\mathbf{M}_u^{-1}(\mathbf{K}_u+\mathbf{K}_t) \end{bmatrix}\begin{bmatrix} \mathbf{q}_s(t) \\ \mathbf{q}_u(t) \end{bmatrix}+\begin{bmatrix} \mathbf{0} \\ \mathbf{M}_u^{-1}\mathbf{K}_t \end{bmatrix}\mathbf{y}(t)+\begin{bmatrix} \mathbf{M}_s^{\dagger}\mathbf{T}^T \\ -\mathbf{M}_u^{-1} \end{bmatrix}\mathrm{sgn}(\mathbf{F}_{MR}) \tag{5}$$

By changing the variables:

$$\begin{cases} \mathbf{z}_1(t)=\begin{bmatrix} \mathbf{q}_s^T(t) & \mathbf{q}_u^T(t) \end{bmatrix}^T \\ \mathbf{z}_2(t)=\begin{bmatrix} \dot{\mathbf{q}}_s^T(t) & \dot{\mathbf{q}}_u^T(t) \end{bmatrix}^T \end{cases}\Rightarrow \dot{\mathbf{z}}_1(t)=\mathbf{z}_2(t) \tag{6}$$

the state space model of differential equation describing the dynamic behavior of full car is obtained:

$$\begin{bmatrix} \dot{\mathbf{z}}_1(t) \\ \dot{\mathbf{z}}_2(t) \end{bmatrix}=\begin{bmatrix} \mathbf{0} & \mathbf{I} \\ \mathbf{K}_z & \mathbf{C}_z \end{bmatrix}\begin{bmatrix} \mathbf{z}_1(t) \\ \mathbf{z}_2(t) \end{bmatrix}+\begin{bmatrix} \mathbf{0} \\ \mathbf{M}_s^{\dagger}\mathbf{T}^T \\ -\mathbf{M}_u^{-1} \end{bmatrix}\mathbf{F}_{MR}+\begin{bmatrix} \mathbf{0} \\ \mathbf{M}_u^{-1}\mathbf{K}_t \end{bmatrix}\mathbf{d}_n(t) \tag{7}$$

The magneto-rheological force $\mathbf{F}_{MR}$ has a non linear expression, that is:

$$F_{MR}=A_f\cdot C_f\cdot 271700\cdot\Phi^{1.5239}\cdot\tanh\left(6.33\times10^{-6}\cdot H\right) \tag{8}$$

where A_f is the active piston surface for magneto-rheological reaction, C_f is the carrier fluid constant, Φ volume fraction of iron particles and H is the induction magnetic field. In the previous expression the only variable that can be changed on line is the magnetic field H .

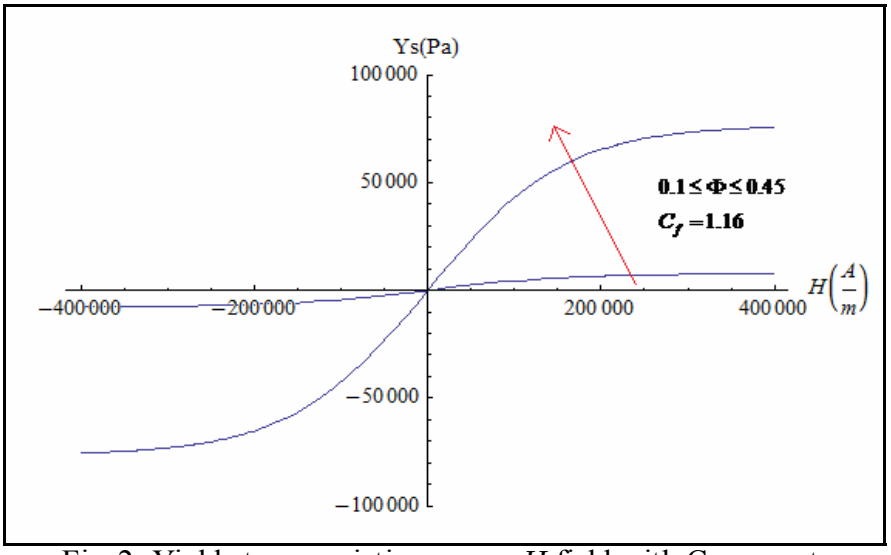

Fig. 2: Yield stress variation versus *H* field with C_f = const.

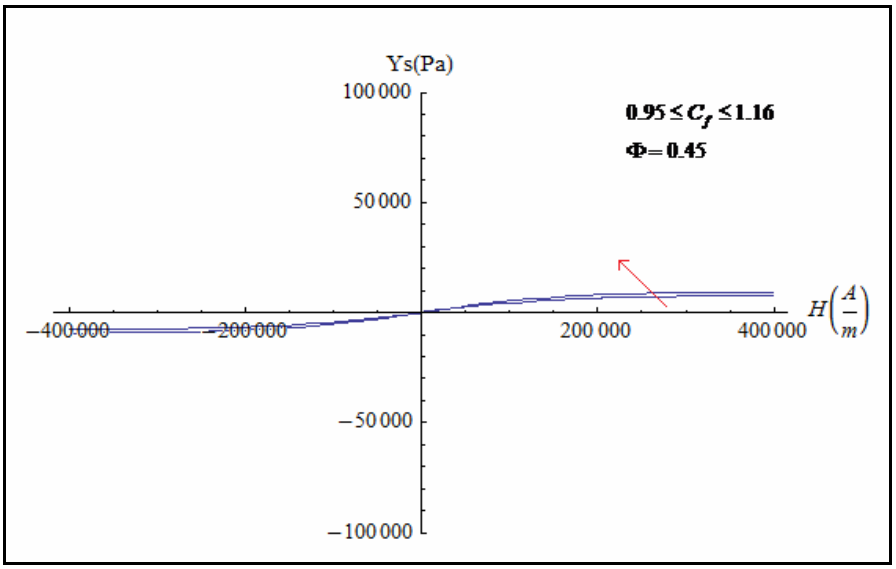

Fig. 3: Yield stress variation versus *H* field with ϕ = const.

The other parameters must be set up during the design of magneto-rheological fluid. These parameters are essential to determine the modulus of the force generated by the magnetic induction field; figures 2 and 3 show the different effect of those parameters. Figure 2 shows that the force for unit of active surface increases by increasing the magnetic induction field, moreover, once fixed a value of C_f , the slope of curve increases by increasing the volume fraction of iron particles. Figure 3 shows that the behavior of yield stress, like a function of magnetic field, is the same of figure 2, but once fixed the value of volume fraction of iron particles the variation of slope is less than in the figure 2. A consequence is that only the variation of iron particle percentage can produce a significant variation of yield stress in order to provide high performance of magneto-rheological damper.

Once the mathematical model is performed, the frequency response of the system is calculated in order to provide some information about the peak of resonances of the system full-car, like figure 4 shows, according the data shown in table 1.

Table 1: Data for simulations of full car

Symbol	Description	S.I.
m_s	mass of vehicle's chassis	$690Kg$
I_y	moment of inertia along y direction	$1222Kg \cdot m^2$
I_x	moment of inertia along x direction	$122Kg \cdot m^2$
m_{fr}	mass of the front right tire	$40Kg$
m_{fl}	mass of the front left tire	$40Kg$
m_{rr}	mass of the rear right tire	$45Kg$
m_{rl}	mass of the rear left tire	$45Kg$
k_{fr}	front right shock absorber stiffness	$17000N/m$
k_{fl}	front left shock absorber stiffness	$17000N/m$
k_{rr}	rear right shock absorber stiffness	$22000N/m$
k_{rl}	rear left shock absorber stiffness	$22000N/m$
c_{fr}	front right shock absorber damping coefficient	$1400Ns/m$
c_{fl}	front left shock absorber damping coefficient	$1400Ns/m$
c_{rr}	rear right shock absorber damping coefficient	$1500Ns/m$
c_{rl}	rear left shock absorber damping coefficient	$1500Ns/m$
k_{tfr}	front right shock absorber tire stiffness	$200000N/m$
k_{tfl}	front left shock absorber tire stiffness	$200000N/m$
k_{trr}	rear right shock absorber tire stiffness	$200000N/m$
k_{trl}	rear left shock absorber tire stiffness	$200000N/m$
a	distance between rear axis and center of mass G	$1.3m$
b	distance between front axis and center of mass G	$1.5m$
c	distance between front left wheel and center of mass G	$1.2m$
d	distance between front right wheel and center of mass G	$1.2m$

Figure 4 is obtained by taking into account the magneto-rheological input F_{MR} for each shock absorber by observing as output the relative displacement between sprung and unsprung mass. The terms sprung mass is inserted into each plot in order to lead the reader the information about the shock absorber excitation. Each plot shows two peaks of resonance produced by the magneto-rheological input that are due to the presence of two masses for each suspension point.

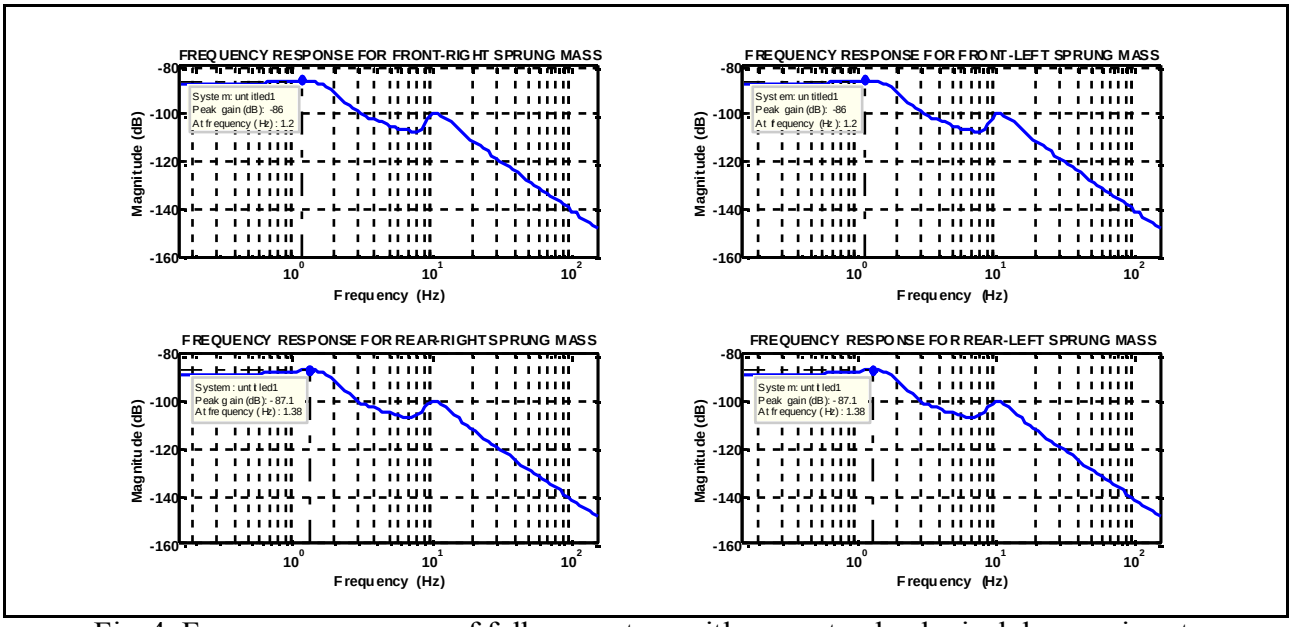

Fig. 4: Frequency response of full car system with magneto-rheological damper input.

In fact, the chassis has a unique body and by considering the constraining located on each corner of that, the sprung mass is carried out. Both sprung and unsprung masses constitute a single system characterized by two degree of freedom. This means that for each shock absorber there is an influence in terms of frequency of the input on the dynamic behavior. In other words if the control input is injected with a certain frequency equals the value of resonance, a permanent oscillation can be induced. This happens only when the speed value exceeds the limit imposed by the user. The introduction of this limit produces a square wave of the magneto-rheological input which is inserted in the mathematical model in a form of conditional instructions as described in the simulations paragraph. This type of control is called switch on/off control. By term passive control is meant the introduction of those components, such as spring and damper, typically used in common shock absorber.

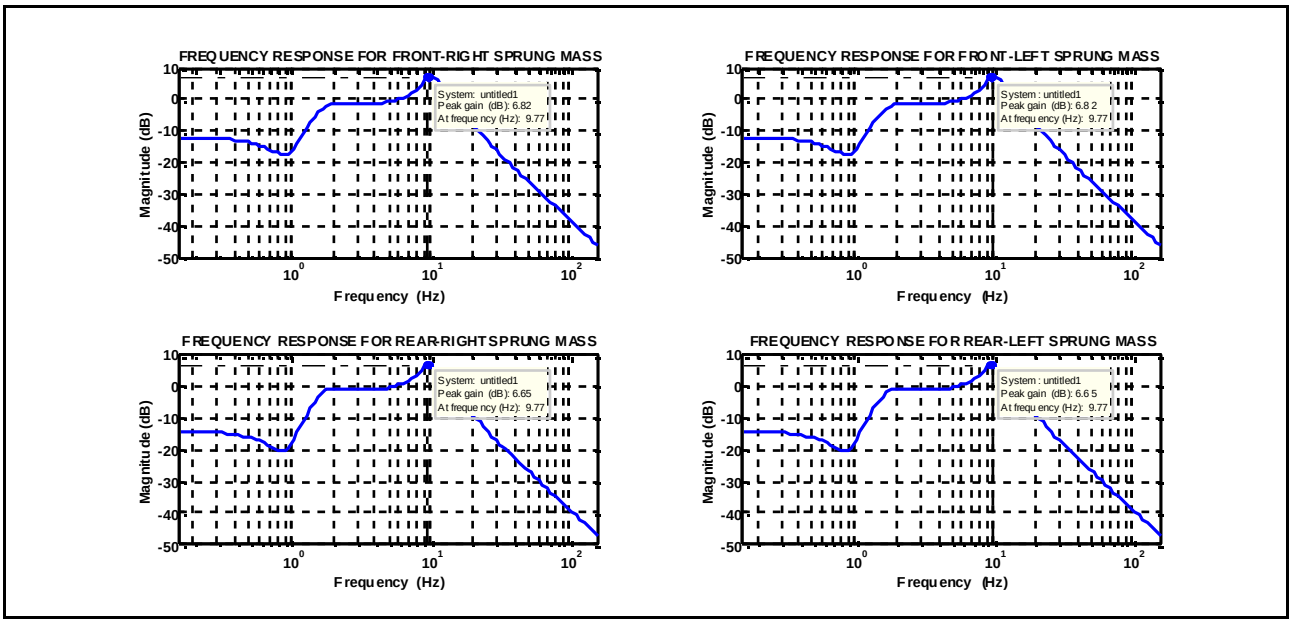

Fig. 5: Frequency response of full car system with road disturbances as input.

Figure 5 shows the frequency response between the road disturbances input and the same output described before or rather the relative displacement in magnitude between the sprung and unsprung mass. All the four plots are characterized by an attenuation of the magnitude while the minimum of Bode's plot is near the value of frequency 10^0Hz. Magnitude increases from this value until to reach the maximum value of the peak, after the magnitude decreases. This decreasing obviously is due to the inertia of the system to follow the signal having high value of frequency.

3. CONTROLLER

A suitable control system must be performed in order to provide a control of damping effect. This control can be realized in different way. The first control of damping is built up a control input generated when the value of speed is greater than an established one [9]. This technique is characterized by the injection of magnetic field with constant value chosen in order to obtain the requested damping effect. According to the mathematical model (12) the vector $\mathbf{F}_{MR}$ has the particular structure so that a road excitation which produces the displacement of unsprung mass does not realize a recalling force on sprung mass but only a dissipation of kinetic energy on it. The algorithm to activate the damping effect is based on the relative speed signal between the sprung and unsprung mass according to relationship (14) because the sensor's position is located in one of the two parts:

$$\begin{cases} c(\dot{x}_s - \dot{x}_u) < 0 \Rightarrow \text{sgn}(\mathbf{F}_{MR}) > 0 \\ c(\dot{x}_s - \dot{x}_u) > 0 \Rightarrow \text{sgn}(\mathbf{F}_{MR}) < 0 \end{cases} \tag{9}$$

This algorithm automatically provides the input signal in order to act on both masses by different direction of magneto-rheological force in the mathematical model.
H-infinity control is the second control system. Its structure is more complicated than the previous controller due to the introduction of all inputs in terms of disturbances and control signal:

$$\mathbf{G} = \begin{bmatrix} \mathbf{A} & \mathbf{B}_1 & \mathbf{B}_2 \\ \mathbf{C}_1 & \mathbf{D}_{11} & \mathbf{D}_{12} \\ \mathbf{C}_2 & \mathbf{D}_{21} & \mathbf{D}_{22} \end{bmatrix} \tag{10}$$

In terms of algebraic blocks scheme, the quarter car plant is considered [MATLab], like figure 6 shows for the open loop:

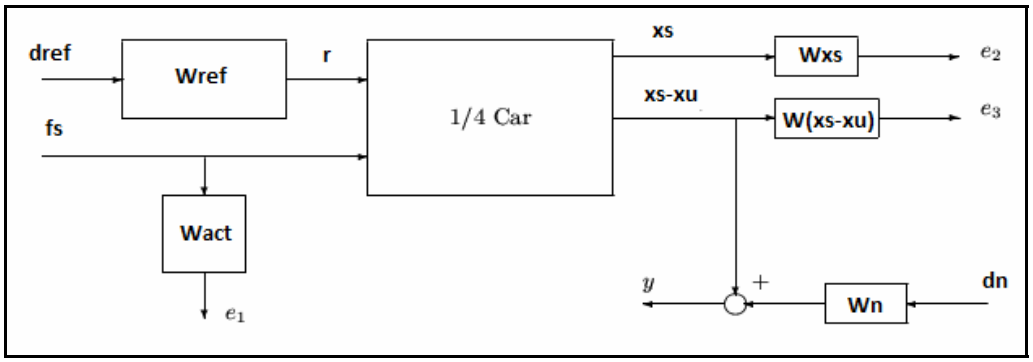

Fig. 6: Dynamic system by algebraic of block scheme of single shock absorber (quarter car).

The weighting functions define the performances of the dynamic system of shock absorber. These functions are relative to the performances of sprung mass displacement, noise input, reference and actuator:

$$W_{xs} = \frac{80\pi}{s+10\pi}; \tag{11}$$

$$W_{act} = \frac{100}{13}\frac{s+50}{s+500}; \tag{12}$$

The introduction of weighting functions in the model (15) increases the order of mathematical model describing the dynamic behavior of full car. This happens because the introduction of new output such as e_1, e_2 and e_3 (fig. 6) that are respectively the maximum magneto rheological admissible force, the displacement of sprung mass, and relative displacement between sprung and unsprung mass. Once the system has new output a new plant is built in order to perform the controller which considers the desired performances required by weighting function. The controller carried out is put in a closed loop with the plant as in the figure 7, [10]:

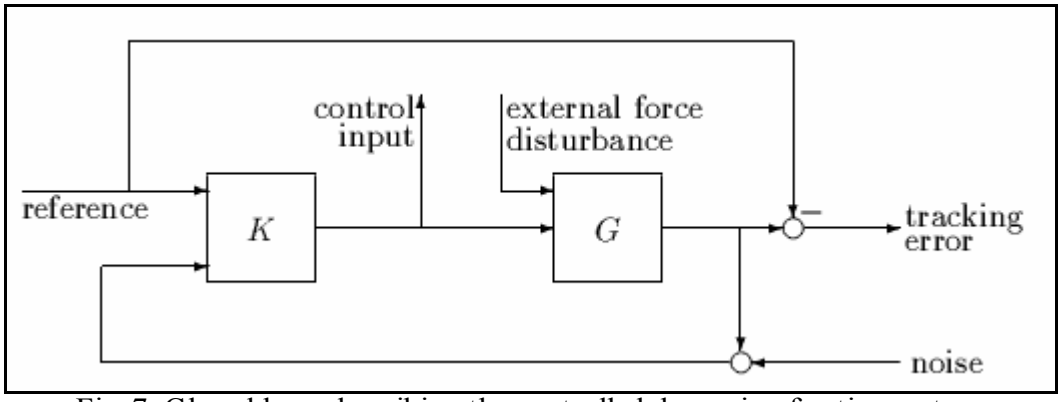

Fig. 7: Closed loop describing the controlled dynamic of entire system.

where the **G** and **K** plant in a feedback produce the new plant in order to develop the following relationship:

$$\begin{bmatrix} r-y(\text{tracking error}) \\ u(\text{control input}) \end{bmatrix} = F(\mathbf{G},\mathbf{K}) \begin{bmatrix} r(\text{reference}) \\ f(\text{external force inside plant } \mathbf{G}) \\ n(\text{noise}) \end{bmatrix} \tag{13}$$

By switch on/off and H-infinity control, the deflection of sprung mass is minimized in order to study the dynamic behavior of entire vehicle by the introduction of the square wave function in the simulations.

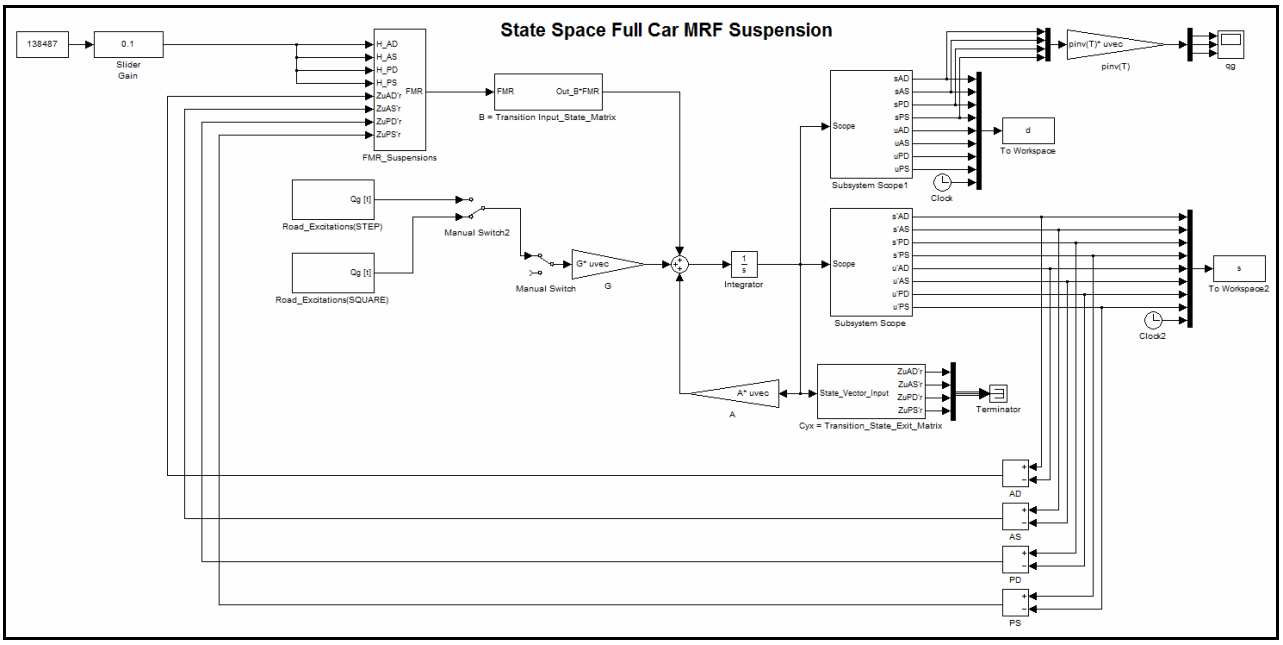

Fig. 8: Simulink Block Scheme of Full Car's dynamic controlled by switch on/off.

4. SIMULATIONS

The first part of this section is characterized by simulations of full car dynamic equipped by switch on/off; the control signal is dependent on the relative speed value between the sprung and unsprung mass. Block scheme for full car model is shown in the figure 8.

The simulations for all the kinds of control systems used in this paper are performed by taking into account an input characterized by square wave having an amplitude of 0.1m with a delay for rear wheels of 0.14s respect the forward wheels, while the car is going ahead with a speed value of 19.4 m/s. The previous data are calculated by considering the distance between the front and rear wheels. Figure 9 shows the block scheme of magneto-rheological force.

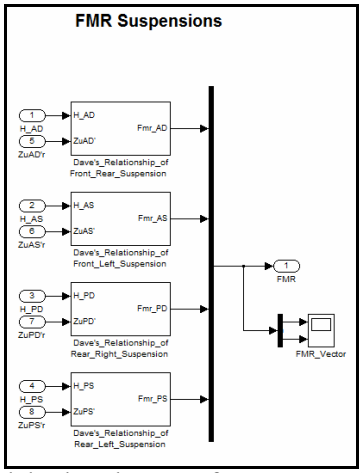

Fig. 9: Simulink block scheme of magneto-rheological force.

Figure 10 shows the conditional instruction to inject the control input of system. Front-right suspension was taken as example in order to provide enough information about the switch on/off operation like *if* block.

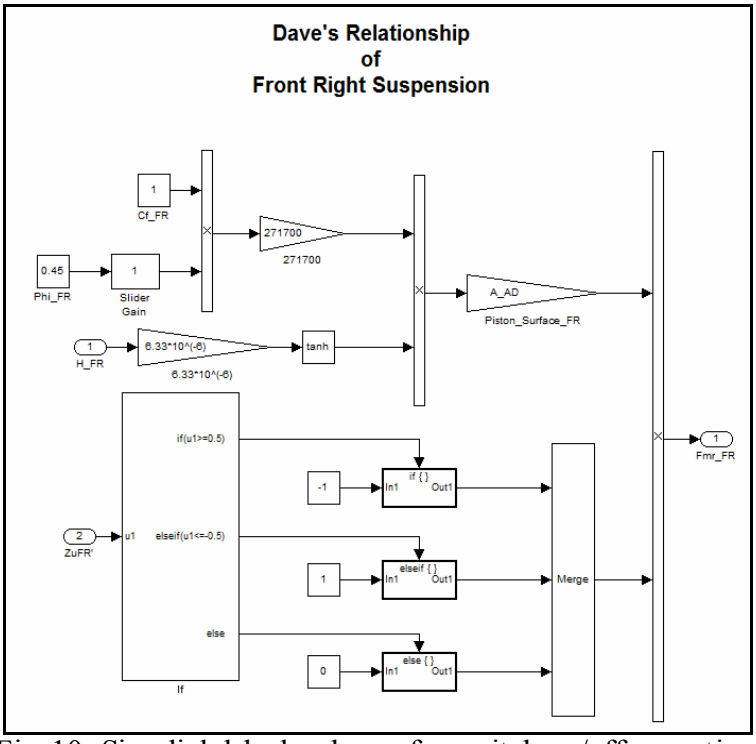

Fig. 10: Simulink block scheme for switch on/off operation.

Figure 11 shows the block scheme of the road disturbances where the relative block to the square wave is connected to the G matrix thanks to a manual switch.
The simulations are performed according the data shown in the Table 1, with the data reported in table 2.

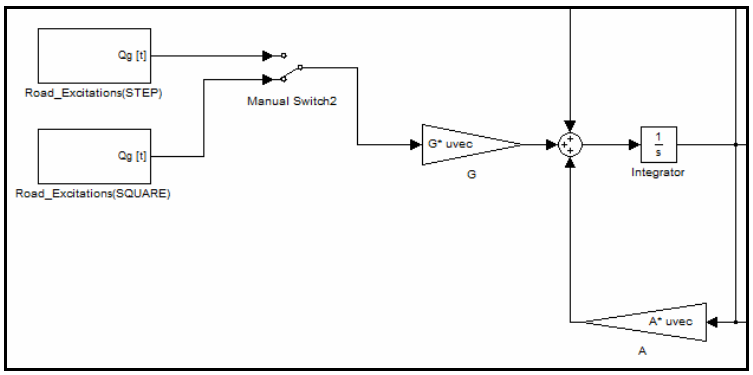

Fig. 11: Simulink block scheme of road disturbances.

Table 2: Data for switch on/off operation of controller

Symbol	Description	S.I.
H	magnetic field	$13848 A/m$
$F_{MR}(H)$	magneto-rheological force	$1050 N$
u_1	speed limit	$\|0.5\| m/s$
d_n	road disturbances(square wave)	$0.1 m$

In the H-infinity control_1, the controller has the form of state space relationship:

$$\begin{aligned}\dot{\mathbf{x}}(t) &= \mathbf{A}_H \mathbf{x}(t) + \mathbf{B}_H \mathbf{u}(t) \\ \mathbf{y}(t) &= \mathbf{C}_H \mathbf{x}(t)\end{aligned} \tag{14}$$

where $\mathbf{u}(t) = \left[\mathbf{x}_s(t) - \mathbf{x}_u(t)\right] \in \mathbb{R}^{4\times 1}$ or rather the difference between the sprung and unsprung mass displacement according to the figure (see controller paragraph). Figure 12 shows Simulink block scheme in order to highlight the substantial differences with the previous one:

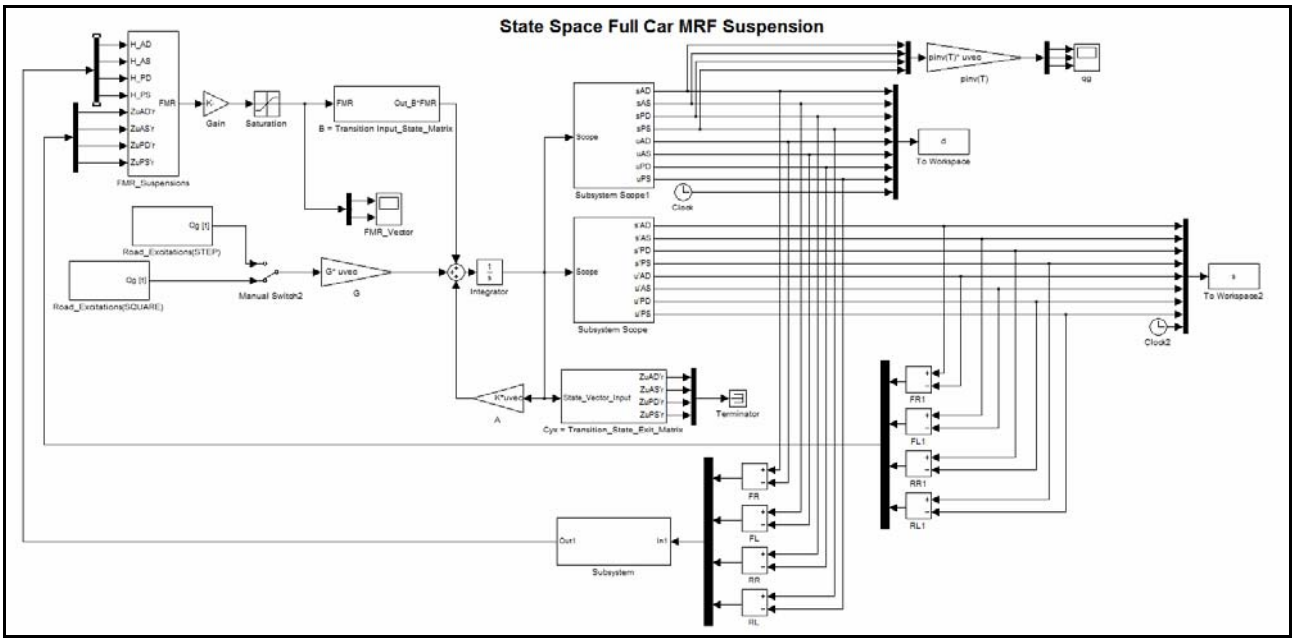

Fig. 12: Simulink Block Scheme of Full Car's dynamic controlled by H-infinity controller.

Figure 13 shows the frequency response of H_∞ controller. The frequency response is calculated for both rear and front shock absorber that are characterized by almost the same value of frequency where the controller generates resonance. Another characteristic is the different response at low frequency where the front damper produces a lower control signal than the rear one. This is due to the different reaction force of the gravity; in fact the center of mass is closer to the rear shock absorber than the front one, so that the output signal of the controller for the rear must be higher than front one:

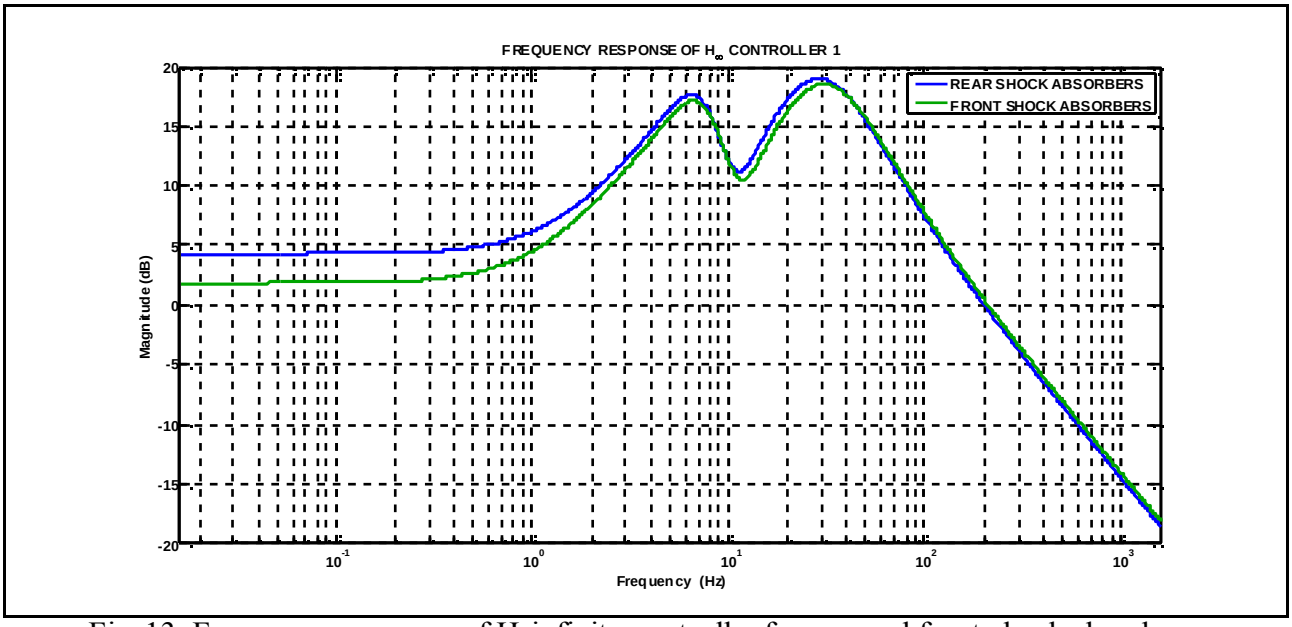

Fig. 13: Frequency response of H-infinity controller for rear and front shock absorbers.

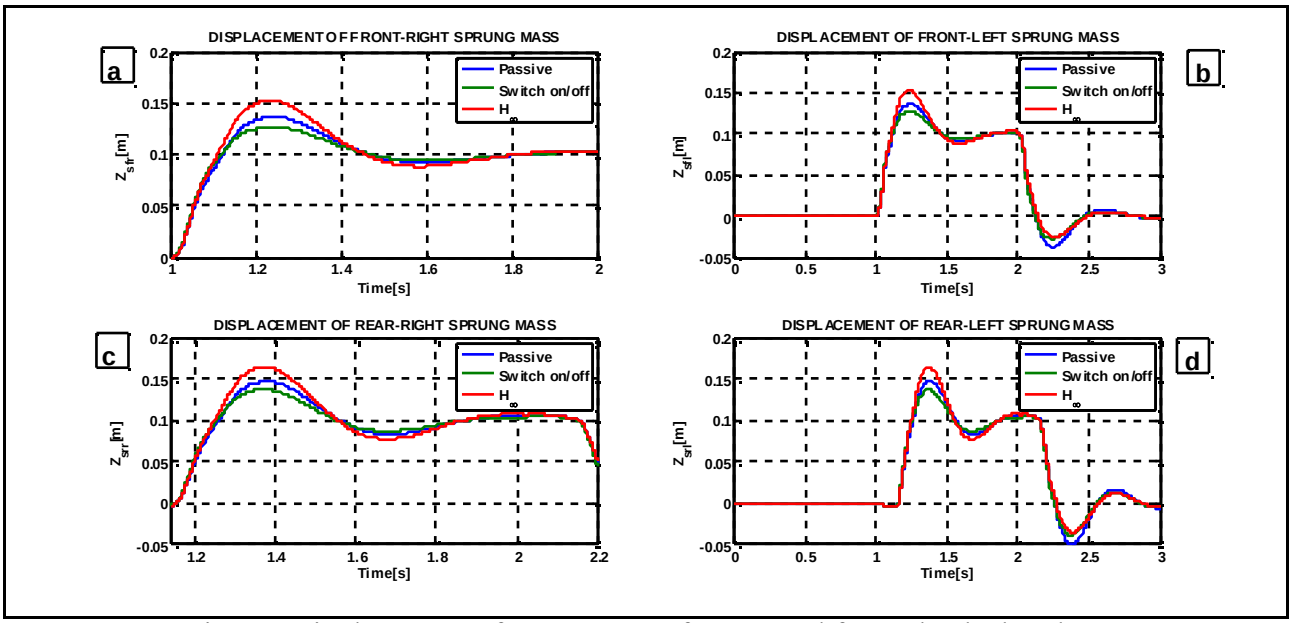

Fig. 14: Displacement of sprung mass for rear and front shock absorber.

Figure 14, 15, 16 and 17 shows the set of simulations to compare the results about the performances offered by the passive, switch on/off and H_∞ controller. They are grouped in displacement results of sprung and unsprung mass respectively and speed. Figure 14a and 14c show the particular about overshoot carried out from the figures 14b and 14d respectively, since the front sprung mass hit on the same time the square wave with the same mechanical properties between right and left shock absorber. The same procedure is maintained for the rear damper and for the others simulations. Figure 14a and 14c show the displacements of sprung mass characterized by different overshoot exhibited by front and rear damper. The overshoot is different according to different controller used, in particular the maximum value is related to H_∞ controller followed by passive dynamic system while the smallest is produced by switch on/off controller. The unsprung mass of front suspension, figure 15a, assumes a different dynamic behavior regard to the sprung mass, in particular the highest displacement of unsprung mass is related to the passive dynamic system followed by H_∞

controller while the smallest one is produce by switch on/off controller. The same behavior is assumed by the rear suspension, figure 15c:

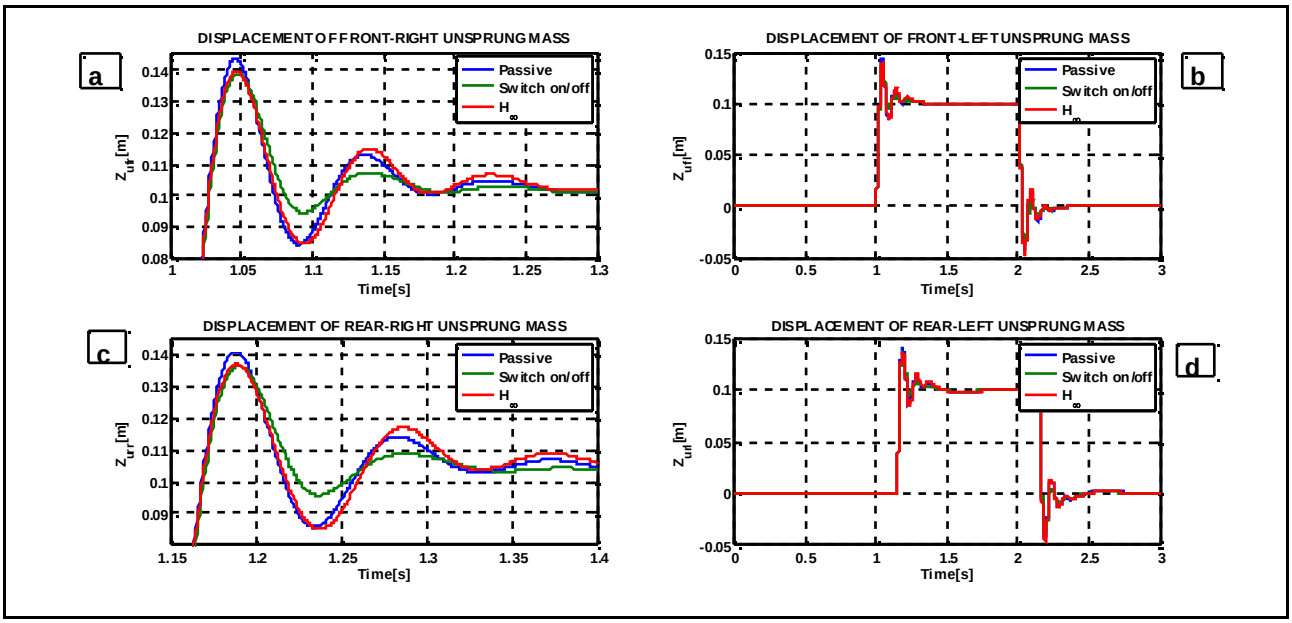

Fig. 15: Displacement of unsprung mass for rear and front shock absorber.

Figures 16 and 17 show the speed signals comparison. In figure 16a the sprung mass exhibits a speed signal whose maximum is obtained with the switch on/off controller followed by H_∞ and passive system. The same behavior is assumed by speed signals of rear suspension, figure 16c.

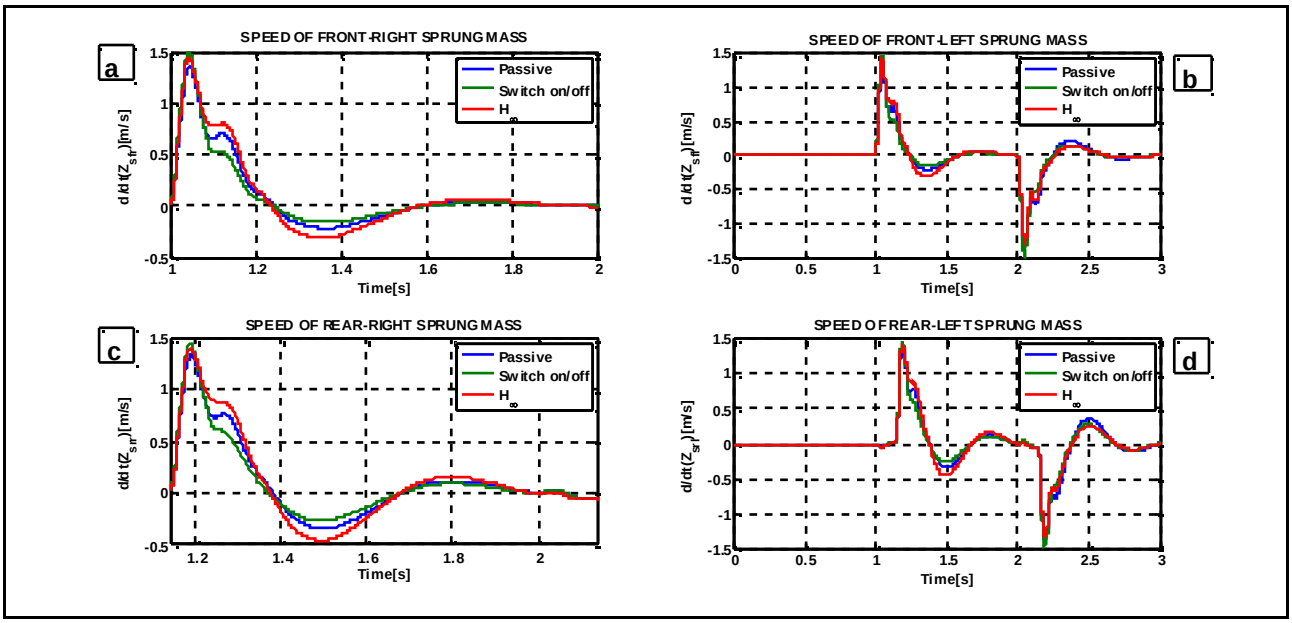

Fig. 16: Speed of sprung mass for rear and front shock absorber.

In the figure 17a the speed of unsprung mass is higher for passive controller than H_∞ while the smaller is produced by switch on/off controller. The same behavior is followed by the rear unsprung mass. There is a difference between the switch on/off and H_∞ controller. This difference is related to the way how the control signal is injected, in particular, when the unsprung mass is excited by square wave, the switch on/off controller produces a square wave, while the H_∞ control produces a proportional control signal to the displacement signal which is characterized by a certain transient

response. This transient, which is typical of dynamic systems, represent obviously a certain delay in the response so that during the excitation of square wave there is a small range of time during which, in presence of H_∞ control, the unsprung mass produces an higher displacement than one exhibited by switch on/off controller.

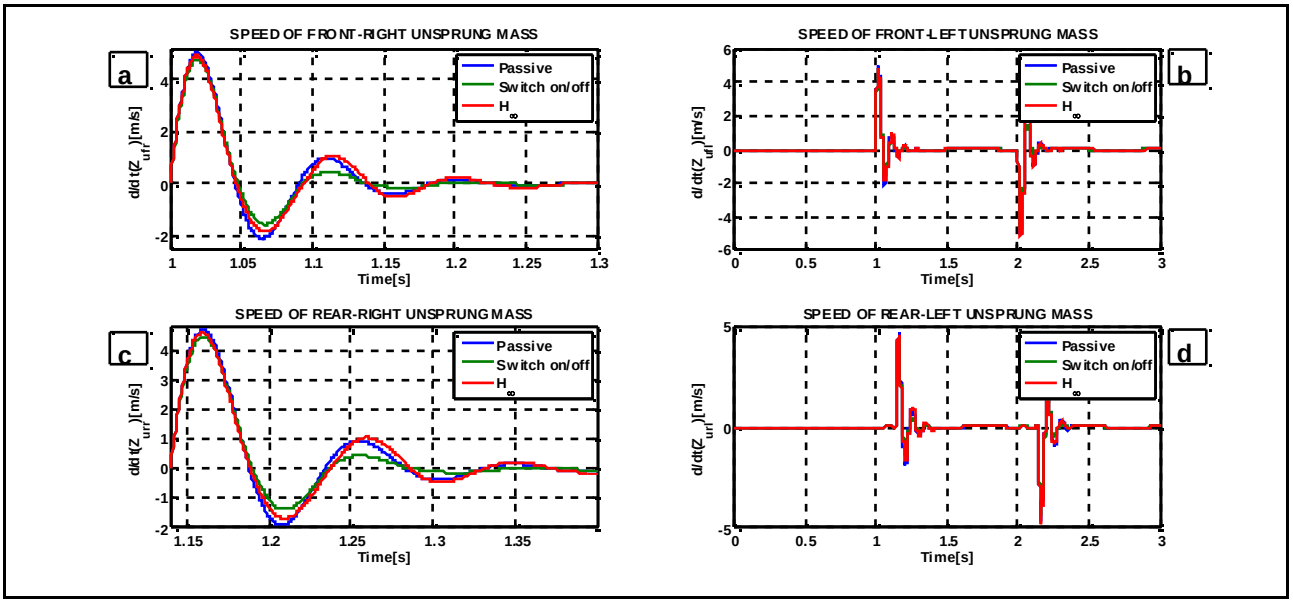

Fig. 17: Speed of unsprung mass for rear and front shock absorber.

5. CONCLUSIONS

In terms of computational burden it's quite difficult to carry out the H_∞ control due to the iterative calculation to get it. Moreover it need of mathematical model of system that in this case is characterized by a set of differential equations. The switch on/off control doesn't need of mathematical model because it is characterized by the injection of input when a certain value of parameter is over the imposed limit; in this case the limit is the relative speed between the sprung and unsprung mass. If a relation with mathematical model exists, it is due to the geometric parameters, such active surface of shock absorber, related the damping coefficient. The substantial differences between the performed controller is the pattern of input signal, in fact, the switch on/off controller provides a square wave signal while the H_∞ control provides a continuous signal. This differences leads the switch on/off controller to exerts the maximum mechanical reaction to the relative displacement while H_∞ control provides a force proportional to the relative displacement. The force is lower than switch on/off one, in fact the figures 17a and 17c show that the displacement of unsprung mass is greater for H_∞ than switch on/off. The consequences is a transferring of high value of force to the chassis characterized by sprung mass and a fast extinction of transient response for both unsprung and sprung mass. The future development are relative to the different introduction of controller such as adaptive control and an active system which provide a dynamic movement of unsprung mass in order to follow the road pattern.

REFERENCES

[1]S. Sassi, K. Cherif, L. Mezghani, M. Thomas and A. Kotrane, "*An innovative magnetorheological damper for automotive suspension: from design to experimental characterization*", Smart Materials and Structures **14** (2005)811-822.

[2]D.C. Batterbee, N.D. Sims, R. Stanway and Z. Wolejza, "*Magnetorheological landing gear: 1. A design methodology*", Smart Materials and Structures **16**(2007)2429-2440.

[3]D.C. Batterbee, N.D. Sims, R. Stanway and M. Rennison, "*Magnetorheological landing gear: 2. Validation using experimental data*", Smart Materials and Structures **16**(2007)2441-2452.

[4]W. Hu, N.M. Wereley, "*Hybrid magnetorheological fluid-elastomeric lag dampers for helicopter stability augmentation*", Smart Materials and Structures **17**(2008)045021(16pp).

[5]R. Stanway, J.L. Sproston and A.K. El-Wahed, "*Applications of electro-rheological fluids in vibration control: a survey"*, Smart Materials and Structures **5**(1996)464-482.

[6]N.D. Sims, N.J. Holmes and R. Stanway, "*A unified modeling and model updating procedure for electrorheological and magnetorheological vibration dampers*", Smart Materials and Structures **13**(2004)100-121.

[7]Y. Kim, R. Langari and S. Hurlebaus, "*Semiactive nonlinear control of building with a magnetorheological damper system*", Mechanical system and Signal Processing **23**(2009)300-315.

[8]H. Hongsheng, W. Jiong, Q. Suxiang and Z. Lijie, "*Research on the Hardware-in-the-Loop Simulation of Magnetorheological Damper Subjected to Impact Load*", Proceeding of the IEEE, International Conference on Automation and Logistics, Qingdao, China September 2008.

[9]G. Barbaraci, P. Ricotta and G.Virzi' Mariotti, (2010). "*Studio del comportamento dinamico di un modello halfcar e confronto fra ammortizzazione passiva e semiattiva a fluido magnetoreologico*". In Atti del XXXIX Convegno Nazionale AIAS. Cosenza .

[10]D.W. Gu, P.Hr. Petkov and M.M. Konstantinov, "*Robust Control Design with* MATLAB", Springer Editions.